Author Manuscript

Author Manuscript

Author Manuscript

Author Manuscript

HHS Public Access

Author manuscript

*J Am Chem Soc*. Author manuscript; available in PMC 2018 May 24.

Published in final edited form as:

*J Am Chem Soc*. 2017 May 24; 139(20): 6911–6918. doi:10.1021/jacs.7b01545.

# Photostable Ratiometric Pdot Probe for in Vitro and in Vivo Imaging of Hypochlorous Acid

**Li Wu**[†,iD], **I-Che Wu**[†], **Christopher C. DuFort**[‡], **Markus A. Carlson**[‡], **Xu Wu**[†], **Lei Chen**[†,iD], **Chun-Ting Kuo**[†], **Yuling Qin**[†], **Jiangbo Yu**[†], **Sunil R. Hingorani**[‡,§,⊥], and **Daniel T. Chiu**[*,†,iD]

[†]Department of Chemistry, University of Washington, Seattle, Washington 98195, United States

[‡]Clinical Research Division, Fred Hutchinson Cancer Research Center, Seattle, Washington 98109, United States

[§]Public Health Sciences Division, Fred Hutchinson Cancer Research Center, Seattle, Washington 98109, United States

[⊥]Division of Medical Oncology, University of Washington School of Medicine, Seattle, Washington 98195, United States

## Abstract

Developing probes for the detection of reactive oxygen species (ROS), a hallmark of many pathophysiological process, is imperative to both understanding the precise roles of ROS in many life-threatening diseases and optimizing therapeutic interventions. We herein report an all-in-one fluorescent semiconducting polymer based far-red to near-infrared (NIR) Pdot nanoprobe for the ratiometric detection of hypochlorous acid (HOCl). The fabrication takes the advantage of flexible polymer design by incorporating target-sensitive and target-inert fluorophores into a single conjugated polymer to avoid leakage or differential photobleaching problems existed in other nanoprobes. The obtained nanoprobe has improved performance in HOCl sensing, such as high brightness, ideal far-red to NIR optical window, excellent photostability, self-referenced ratiometric response, fast response, and high selectivity. The dual-emission property allows the sensitive imaging of HOCl fluctuations produced in living macrophage cells and peritonitis of living mice with high contrast. This study not only provides a powerful and promising nanoprobe to be potentially used in the investigations of in situ HOCl status of diseases in living systems but also puts forward the design strategy of a new category of ratiometric fluorescent probes facilitating precise and reliable measurement in biological systems.

[*]**Corresponding Author**. chiu@chem.washington.edu.

**ORCID**

Li Wu: 0000-0002-4118-7970

Lei Chen: 0000-0001-6159-0137

Daniel T. Chiu: 0000-0003-2964-9578

**ASSOCIATED CONTENT**

**Supporting Information**

The Supporting Information is available free of charge on the ACS Publications website at DOI: 10.1021/jacs.7b01545.

Experimental conditions, supplementary methods for chemical synthesis and characterization of compounds, supplementary experiments and data (PDF)

The authors declare no competing financial interest.

Author Manuscript Author Manuscript Author Manuscript Author Manuscript

## Graphical Abstract

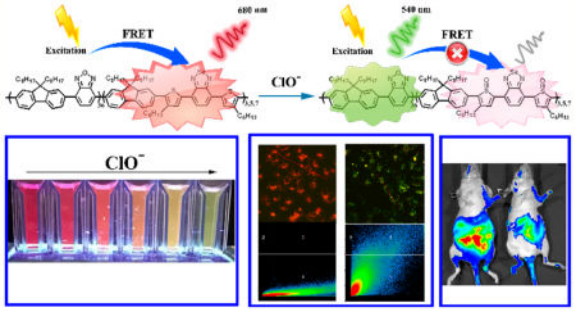


## INTRODUCTION

Reactive oxygen and nitrogen species (ROS and RNS, respectively) are essential signaling molecules that mediate many biological events in a variety of physiological processes. They are also implicated in various pathophysiological processes, including aging, autoimmunity, cancer, chronic inflammatory diseases, and neurodegenerative disorders.[1–5] Hypochlorous acid (HOCl) is a ROS of particular interest. HOCl is biologically generated by an oxidation reaction between hydrogen peroxide ($H_2O_2$) and chloride ions ($Cl^-$) under the catalysis of myeloperoxidase (MPO) within phagosomes.[6,7] Endogenous HOCl is a powerful natural oxidant that can react with proteins, DNA, RNA, fatty acids, and cholesterol and is thought to play vital physiological roles in living systems.[8,9] On the one hand, HOCl has microbicidal activity and is beneficial for innate host defense during microbial invasion.[10,11] On the other hand, oxidative stress resulting from uncontrolled production of HOCl within phagocytes may lead to an adverse effect on host physiology; HOCl is known to be closely related to the progression of numerous human diseases.[12,13]

Despite its importance, however, HOCl's precise roles in biological activities remain elusive. Thereby, the development of accurate and reliable analytical methods for monitoring biological HOCl in living systems is very important to elucidate its physiological functions. Fluorescence imaging is useful for sensing biomolecules in living systems because of its unique advantages of excellent sensitivity and selectivity, high spatial and temporal resolution, simplicity of implementation, facile visualization, and real-time analysis of intracellular dynamics and biomolecular localization at subcellular levels.[14,15] In the past few years, a number of fluorescent probes have been designed to clarify the function of HOCl in organisms and were based on the most versatile fluorophores,[15,16] including coumarin,[17] fluorescein,[18] rhodamine,[19–21] cyanine,[22–24] boron-dipyrromethene (BODIPY),[25,26] ruthenium(II),[27] iridium(III),[28,29] and lanthanide complexes.[30] Although these probes had their uses for in vitro and in vivo imaging, problems with them, such as the lack of selectivity, poor water-solubility, prolonged oxidation reaction time, and low stability due to autoxidation and photobleaching, largely limited their application. Furthermore, most of these were synthetic-dye-based, small-molecule fluorescent probes that report HOCl with only "turn-on" or "turn-off" changes in the intensity of a single emission band (Table S1, small molecules). Because these probes are not ratiometric and lack internal reference, their operations were often hampered by issues such as fluctuation of instrumental parameters,

Author Manuscript Author Manuscript Author Manuscript Author Manuscript

variations in microenvironment around the probe molecule, probe distribution, and photobleaching.

In contrast, ratiometric fluorescent probes report analyte-induced emission intensity changes at two or more different wavelengths to provide built-in self-calibration for correction of a variety of analyte-independent factors and to increase the dynamic range of fluorescence measurement.[31,32] Like the internal reference approach used in many other analytical methods, ratiometric sensing features increased signal-to-noise ratio and thus more reliable quantification.

With the rapid emergence of nanotechnology, hybrid nanostructures with intrinsic fluorescence have been widely used to fabricate ratiometric bioimaging probes for measurements of HOCl levels[29,33–36] (Table S1, nanoprobe). However, most of these ratiometric sensors suffered from poor selectivity, impeding the practical application for the profiling of an individual ROS. Furthermore, the rate of photobleaching was very different between conjugated target-sensitive fluorophores and nanoparticle matrix. There also was the worry of leakage of the fluorophores from the interior or inner region of the nanomaterial matrix from those nanoparticles made by physical entrapment method. Problems like these could lead to erroneous measurements based on the ratio between the emission intensity of sensing and reference fluorophores. Taking the above situations into consideration, developing a new ratiometric fluorescent probe with improved properties, including fast response, high brightness, good photostability, enhanced sensitivity and selectivity for HOCl, and suitability for biological applications, is still much needed to meet the requirements of precise and quantitative analysis of HOCl in living systems with a straightforward and visual mode.

Semiconducting polymer dots (Pdots), composed of one or more types of conjugated polymers, have become a class of promising fluorescent probes in biology, chemistry, and material-science fields. Their attributes include easy preparation, high brightness, excellent photostability, high quantum yield, good water solubility, excellent biocompatibility, and passive targeting capacity to tumors or inflammation areas by enhanced permeability and retention (EPR) effect.[37–39] Significant advancements in biological applications of Pdots have been made recently in biological/chemical sensors, fluorescence imaging, and gene and drug delivery.[38,40–46] To date, however, the application of Pdots for ROS sensing remains largely unexplored. Compared with other fluorescent probes, a probe based on Pdots could offer increased imaging contrast accuracy and high stability for long-term observations.[23,47–50] Pdots are even more useful for exploiting ratiometric fluorescence sensing as their tunable fluorescence emission band permits facile design of Pdots for ratiometry in the terms of fluorescence resonance energy transfer (FRET).[44,51]

Here, we report an all-in-one fluorescent conjugated polymer $PFOBT_{36}SeTBT_{x}$ based far-red to near-infrared (NIR) Pdot for the ratiometric detection of $ClO^-$ in living cells and inflammatory microenvironments in living mice. $PFOBT_{36}SeTBT_{x}$ is designed to comprise a $ClO^-$-inert component, benzoxadiazole (OBT), as the energy donor and a $ClO^-$-sensitive fluorophore, 4,7-bis(2-thienyl)-2,1,3-benzoselenadiazole (SeTBT), as the energy acceptor, to enable FRET from the OBT part to the fluorophore SeTBT in the absence of $ClO^-$ (Scheme

Author Manuscript Author Manuscript Author Manuscript Author Manuscript

1). The presence of $ClO^-$ can oxidize energy-accepting fluorophore SeTBT and subsequently disturb the FRET process within $PFOBT_{36}SeTBT_x$ Pdots, ultimately leading to an enhanced emission of OBT in green channel and an attenuated emission of SeTBT in far-red to NIR channel. The incorporation of the target-inert and -sensitive fluorophores into an all-in-one conjugated polymer to form the homogeneous nanoprobe can eliminate some of the issues of leakage or differential photobleaching when ratiometric measurements are performed. The use of far-red to NIR emission also minimizes the background fluorescence with less scattering, penetrates deeper into tissues, and is far less likely to damage the living systems. Importantly, with excellent photostability and good biocompatibility, the designed Pdots-based nanoprobe allows sensitive and selective imaging and monitoring of $ClO^-$ both in living cells and in the microenvironment of local inflammation in live animals with high contrast.

## RESULTS AND DISCUSSION

### Synthesis and Characterizations of HOCl Probes

The Pdots of $PFOBT_{36}SeTBT_x$ polymers (*x*: different molar ratios of SeTBT in the copolymer) were prepared by the nanoprecipitation method described in our previous report.[46,52] Briefly, to form the fluorescent Pdots, the semiconducting polymer $PFOBT_{36}SeTBT_{3,5,7}$ (see Scheme 1 for the chemical formula) was co-condensed with a small amount of the amphiphilic polymer carboxyl-functionalized polystyrene-*g*-poly(ethylene oxide) (PS-PEG-COOH). During nanoparticle formation, the hydrophobic polystyrene backbone of PS-PEG-COOH were most likely embedded inside the Pdots, while the hydrophilic PEG chains and functional carboxyl groups extended out into the aqueous environment. By virtue of the above nanoarchitecture, the as-synthesized Pdots possess desirable advantages over small molecules, including good water solubility and resistance to nonspecific absorption with a biocompatible PEG layer.

The size of obtained $PFOBT_{36}SeTBT_x$ Pdots was characterized by transmission electron microscopy (TEM) and dynamic light scattering (DLS). As shown in Figure 1A–C, the Pdots were mostly spherical and dispersed rather evenly on the grid surface. The average size of $PFOBT_{36}SeTBT_3$, $PFOBT_{36}SeTBT_5$, and $PFOBT_{36}SeTBT_7$ Pdots were 22.83 ± 1.086 nm, 23.52 ± 0.9815 nm, and 22.94 ± 1.556 nm, respectively (Figure 1A–C, inset, and Table S2). There were no obvious changes in nanoparticle size and shape when tuning the composition of $PFOBT_{36}SeTBT_x$ copolymer by changing the molar ratio of the target-sensitive SeTBT part. Absorption and fluorescence spectroscopy were further performed to investigate the optical properties of $PFOBT_{36}SeTBT_x$ Pdots. As indicated in Figure 1D, the absorption peaks at 400–500 nm and 550–650 nm are attributed to the OBT units and SeTBT in the copolymers, respectively. Upon excitation of PFOBT, $PFOBT_{36}SeTBT_x$ Pdots exhibited an obvious emission peak at 680 nm, confirming the excellent energy transfer from OBT to SeTBT. The intensity ratio of SeTBT absorption peak to the OBT absorption peak increased with the increasing feeding ratios of SeTBT monomers, while their corresponding emission intensities in the far-red to NIR spectral region were dramatically decreased. Since the sensing performance of the ratiometric nanosensor, such as sensitivity and detection range, is affected by the ratio between target-sensitive and -inert parts in a single Pdot, there

Author Manuscript Author Manuscript Author Manuscript Author Manuscript

is a trade-off between QY and molar ratio of $ClO^-$-sensitive unit SeTBT for the design of Pdot-based ratiometric $ClO^-$ sensor.

## Fluorescent Response of As-Synthesized Pdots to HOCl

The fluorescence responses of $PFOBT_{36}SeTBT_x$ Pdots toward $ClO^-$ were first evaluated to find the best candidate. $PFOBT_{36}SeTBT_x$ had high pH stability in a wide range of proton concentrations (Figure S5) and high photostability (Figure S6), which facilitated its performance in long-term experiments in living cells. Figure 2A,C,G shows the representative fluorescence spectral changes of $PFOBT_{36}SeTBT_3$, $PFOBT_{36}SeTBT_5$, and $PFOBT_{36}SeTBT_7$ Pdots upon addition of $ClO^-$, respectively. With increasing concentrations of $ClO^-$, the emission spectrum changed dramatically with a large decrease in emission at 680 nm and a concomitant increase in emission at 540 nm, resulting in ratiometric detection of $ClO^-$. The QY of $PFOBT_{36}SeTBT_3$, $PFOBT_{36}SeTBT_5$, and $PFOBT_{36}SeTBT_7$ Pdots recorded at the region of 560–900 nm decreased from 16.7 to 8.6, from 13.6 to 7.3, and from 9.3 to 4.9 in the presence of 500 uM $ClO^-$, respectively, while the corresponding QY recorded at the region of 490–560 nm increased (Table S2), which indicated that FRET between OBT and SeTBT unit was disrupted and that the donor fluorescence (OBT) at 540 nm was recovered. The fluorescence intensity ratio between 540 and 680 nm of $PFOBT_{36}SeTBT_5$ Pdots ($R = I_{540nm}/I_{680nm}$, relative variation: $(R - R_0)/R_0$; where $R_0$ indicates the fluorescence intensity ratio of pure Pdots in the absence of $ClO^-$ and $R$ is the fluorescence intensity ratio with different $ClO^-$ concentrations) exhibited a much larger enhancement compared to those of $PFOBT_{36}SeTBT_3$ and $PFOBT_{36}SeTBT_7$ Pdots upon the addition of $ClO^-$ (Figure 2B,D,E,H–I), illustrating a superior sensitivity in detecting $ClO^-$. In addition, the large ratiometric variation also allowed the clear visualization of the solution's fluorescent color change. In the absence of $ClO^-$, the solution fluorescent color was red, which turned to orange when the concentration of $ClO^-$ was 100 μM (Figure 2F). With the further increase in $ClO^-$ concentrations, the emission color turned to yellow and finally to green at the concentration of 500 μM. The distinguishable emission color variation at different $ClO^-$ concentrations enabled quantification of $ClO^-$ by the naked eye. On the basis of our analyses, $PFOBT_{36}SeTBT_5$ Pdots was chosen as the $ClO^-$ sensing probe for the following experiments. The maximum ratio enhancement could reach more than 40-fold when $ClO^-$ concentration was above 250 μM (Figure 2E). The emission intensity ratio changes showed an excellent linear relationship with $ClO^-$ concentrations in the wide ranges of 0–50 μM and 50–250 μM, respectively (Figure 2D,E). The detection limit of $PFOBT_{36}SeTBT_5$ Pdots for $ClO^-$ was determined to be as low as 0.5 μM. Additionally, the results of the reaction kinetics demonstrated that the reaction of $PFOBT_{36}SeTBT_5$ Pdots with $ClO^-$ caused a large time-dependent fluorescence intensity ratio change, which was completed within 2 min (Figure S7), suggesting a fast reaction between the Pdot probe and $ClO^-$. We also verified the sensing performances of $PFOBT_{36}SeTBT_5$ Pdots toward $ClO^-$ in acidic and basic solutions. As shown in Figure S8, strong enhancement of fluorescence intensity ratio $I_{540nm}/I_{680nm}$ was observed during titration of $ClO^-$ to $PFOBT_{36}SeTBT_5$ Pdot solutions of pH 5, 6, and 9, which clearly indicate that this probe can be used in a broad range of pH values.

Author Manuscript Author Manuscript Author Manuscript Author Manuscript

The fluorescence responses of $PFOBT_{36}SeTBT_5$ Pdots in the presence of various potentially interfering species, including highly active oxidizing and reducing species, were tested. As shown in Figure 3A,B, $ClO^-$ triggered an obvious spectral change and a remarkable enhancement of emission ratio $I_{540nm}/I_{680nm}$, while spectral or emission ratio changes by other ROS or active reducing species up to 1 mM were not discernible. Furthermore, a red-to-orange solution fluorescent color change could be directly visualized by the naked eye for $PFOBT_{36}SeTBT_5$ Pdots after incubation with $ClO^-$ (Figure 3B, inset). In contrast, various other potentially interfering substances of higher concentration did not result in any visible fluorescent color changes even after incubation overnight. In short, these results indicate the high selectivity of the $PFOBT_{36}SeTBT_5$ Pdots for $ClO^-$ analysis. This desirable selectivity could be ascribed to the oxidation-based mechanism of fluorescence quenching such that nonoxidants, weak oxidants, and reductants in the system exert minimal interference with the fluorescence responses.

## Mechanism of Pdot Nanoprobe Responding to HOCl

We hypothesized the detection mechanism of $PFOBT_{36}SeTBT_5$ Pdots toward $ClO^-$ was the oxidation of energy-accepting fluorophore SeTBT that subsequently disturbed the FRET process within $PFOBT_{36}SeTBT_5$ Pdots (Scheme 1), which was in agreement with literature precedents.[50,53,54] To further investigate the reaction mechanism, we performed mass spectrometry to study the structural variations of SeTBT after reaction with $ClO^-$. The structure of the detection product, oxidized SeTBT, was unambiguously confirmed by MALDI-TOF ($[M]^+ = m/z$ 549.886) (Figure S9). Optical spectroscopy results further supported this hypothesis. PFOBT Pdots, composed of the same component as the energy donor part in $PFOBT_{36}SeTBT_5$ Pdots (Figure S10, inset), were inert toward $ClO^-$ (Figure S10). Figure S11 shows the normalized absorption of $PFOBT_{36}SeTBT_5$ Pdots in PBS solution with different amounts of $ClO^-$. The relative absorbance intensity of SeTBT monomer at around 580 nm was continuously attenuated with the increased concentration of $ClO^-$, confirming the oxidation of SeTBT monomer by $ClO^-$.

To further confirm the proposed mechanism, we prepared another two kinds of Pdots, PFDHTBOT (Figure S12A) and PFDHTBT (Figure S13A), with emitter structures similar to that of SeTBT. Fluorescence titration of a solution of PFDHTBOT or PFDHTBT Pdots with $ClO^-$ both demonstrated a decrease of the absorbance intensity and fluorescent emission (Figures S12B–D and S13B–D), which strongly supported the oxidation mechanism proposed here.

## Visualizations of HOCl in Cells

To evaluate the ability of the probe to image the $ClO^-$ in biological systems, we first investigated the cytotoxicity and photostability of $PFOBT_{36}SeTBT_5$ Pdots. The MTT assays were performed in MCF-7 cells and Raw 264.7 cells (Figure S14). MTT results show that the materials possessed good biocompatibility in living cells, which was necessary to demonstrate before developing any further potential biomedical applications. Photostability tests in living cells demonstrated that $PFOBT_{36}SeTBT_5$ Pdots in MCF-7 cells was highly resistant to photobleaching compared to the commercial dye FITC (Figure S15) and

Author Manuscript Author Manuscript Author Manuscript Author Manuscript

phycoerythrin (PE) (Figure 4 and Figure S16), indicating that $PFOBT_{36}SeTBT_5$ Pdots had sufficient photostability for biological imaging and sensing.

After confirming the sensitivity, selectivity, biocompatibility, and photostability of the probe, we next explored the potential application of $PFOBT_{36}SeTBT_5$ Pdots for imaging $ClO^-$ in vitro. Probe-treated MCF-7 cells were incubated with PBS and various concentrations of $ClO^-$, respectively. After 30 min, fluorescence signals in the green (530–600 nm) and far-red (>650 nm) channels were collected with the excitation wavelength of 405 nm. As shown in Figure 5A, MCF-7 cells loaded with $PFOBT_{36}SeTBT_5$ Pdots treated with only PBS solution displayed intense red and weak green luminescence. Additionally, the intensity profile of the linear region of interest across the cell and the scatter plot clearly illustrate the relative fluorescence intensity collected from the two channels. However, longer incubation of the cells with NaClO showed an increased fluorescence of green channel and a relatively attenuated fluorescence of red channel. These changes were accompanied by a dramatic color change of merged channel from red to yellow with the increased concentration of NaClO (Figure 5B–E) or increased incubation time (Figure S17), in good agreement with the $ClO^-$-elicited ratiometric fluorescence response. Notably, the scatter plot of the green and red channels clearly showed that the dominance of the intracellular fluorescence was shifted from red to green upon incubation with increased amounts of NaClO; the changes in the intensity profiles of the linear region of interest across the cell were synchronous in the two channels (Figures 5 and S17). Flow cytometry is a quantitative cellular analysis technique that provides rapid analysis of multiple characteristics of single cells. To confirm further the excellent probe performance seen in confocal imaging, we also explored the application of the Pdot nanosensor in flow cytometry. As can be seen in Figure S18, fluorescence intensity of the green channel increased as a function of NaClO concentration (Figure S18C), while the fluorescence intensity obtained from the red channel decreased (Figure S18B).

Because the distribution of cell populations in the scatter plot represents the ratio of the red/green channel values, monitoring $OCl^-$ levels in different cell samples could be readily achieved by comparison of the relative distributions of the cell populations in flow cytometry (Figure S18A). These results established the feasibility of $PFOBT_{36}SeTBT_5$ Pdots for both the fluorescence imaging and flow cytometric analysis of exogenous HOCl in cells in a ratiometric mode.

## Determinations of Endogenous HOCl

Inspired by the desirable results of sensing exogenous HOCl in the MCF-7 cells, we then attempted to test the capability of the nanoprobe to image endogenously generated HOCl in cultured cell types involved in inflammation. To mimic the inflammatory condition that activates resting tissue macrophages, the murine cell line RAW264.7 was chosen to produce endogenous HOCl upon culturing with lipopolysaccharide (LPS) and phorbol 12-myristate 13-acetate (PMA). Raw 264.7 cells stained with the nanoprobe $PFOBT_{36}SeTBT_5$ Pdots demonstrated a strong fluorescence in the far-red channel, while negligible fluorescence was observed in the green channel (Figure 6A). After the stimulation treatment with LPS and PMA, a significant enhancement in the green fluorescence and obvious color change from

Author Manuscript Author Manuscript Author Manuscript Author Manuscript

red to orange in merged channel were observed (Figure 6B). The observation indicated the activation of the Pdot nanoprobe by HOCl under conditions of inflammation. Furthermore, the scatter plot was also shifted from the red to the green channel, which was consistent with the results of the intensity profiles of the linear region (Figure 6B). To verify that the fluorescence enhancement response at the green channel in Figure 6B originated from the action of HOCl in cells, we performed a control experiment by treating the probe-loaded cells with *N*-acetyl-L-cysteine (NAC), a powerful free-radical scavenger with high membrane permeability, along with LPS and PMA stimulation.[55] As expected, no obvious fluorescence change was observed (Figure 6C), indicating that NAC scavenged endogenously produced HOCl from RAW264.7 cells and effectively inhibited the activation of Pdot probe. Moreover, another control experiment was carried out by treating macrophage cells loaded with $PFOBT_{36}SeTBT_5$ Pdots with 4-aminobenzioc hydrazide (ABAH), a myeloperoxidase inhibitor known to prevent the formation of hypochlorous acid.[56] A similar green fluorescence-inhibiting effect by ABAH was observed in RAW264.7 cells (Figure 6D), further supporting the idea that the activation of the Pdot probe arose from the selective response to native HOCl. Similar results were obtained from flow cytometric analysis (Figure S19), demonstrating that endogenous HOCl production in RAW264.7 cells can be readily detected in flow cytometry by using $PFOBT_{36}SeTBT_5$ Pdots as fluorescent probes.

## Profiling HOCl in Living Mice

Having performed the $ClO^-$ imaging in living cells, the $PFOBT_{36}SeTBT_5$ Pdots nanoprobe was next applied to the imaging of HOCl in living mice. First, we checked the fluorescence performance of the Pdot nanoprobe using an in vivo imaging system. As shown in Figure 7A, the ratio obtained by pixel-by-pixel calculation of images recorded in the red and green channels of the in vivo imaging system decreased as the concentration of $ClO^-$ increased. This observation was consistent with the previous spectral results. The feasibility of the $PFOBT_{36}SeTBT_5$ Pdots for the in vivo imaging of $ClO^-$ was next evaluated by detecting the fluorescence of $PFOBT_{36}SeTBT_5$ Pdots activated by exogenous $ClO^-$ in live mice. The optical images were acquired after subcutaneous injection of a solution of $PFOBT_{36}SeTBT_5$ Pdots in saline (left) or $ClO^-$ (right) into the dorsal area of nude mice. As shown in Figure 7B, the value of the fluorescence intensity ratio $I_{red}/I_{green}$ of $PFOBT_{36}SeTBT_5$ Pdots in the presence of $ClO^-$ was much lower than that of the $PFOBT_{36}SeTBT_5$ Pdots treated with saline, suggesting the ability of $PFOBT_{36}SeTBT_5$ Pdots to detect the exogenous $ClO^-$ in living mouse.

Subsequently, the in vivo imaging of endogenous $ClO^-$ using $PFOBT_{36}SeTBT_5$ Pdots was tested in live mice that were a model for peritonitis that was induced by intraperitoneal (i.p.) injection of LPS. As shown in Figure 7C, the mouse on the right was treated with LPS to induce inflammation; the mouse on the left treated with saline acted as control. After the injection of $PFOBT_{36}SeTBT_5$ Pdots, the mouse with inflammation showed a decreased fluorescence intensity ratio $I_{red}/I_{green}$, indicating that the Pdot nanoprobe was suitable for ratiometric imaging of $ClO^-$ in live animals. Compared with the recently reported probes for the detection of $ClO^-$ (Table S1), the dual-emission property of the Pdot nanoprobe allowed for the sensitive imaging of the $ClO^-$ in cells and peritonitis in mice with high contrast, which was superior to the performance of most of the reported probes.

Author Manuscript Author Manuscript Author Manuscript Author Manuscript

## CONCLUSION

We have developed a far-red to NIR ratiometric fluorescent HOCl probe, $PFOBT_{36}SeTBT_5$ Pdot, which was based on an all-in-one fluorescent conjugated polymer. The Pdot probe had high brightness, excellent photostability, and good water solubility. We rationally designed the ratiometric probe by incorporating target-sensitive and -inert fluorophores into a single conjugated polymer to form a homogeneous nanoprobe to avoid leakage or differential photobleaching problems and to improve the performance of the ratiometric probe. The reaction of the Pdot probe with HOCl disrupted the FRET process between energy donor OBT and energy accepting fluorophore SeTBT, resulting in a large change in the emission spectrum. $PFOBT_{36}SeTBT_5$ Pdots demonstrated not only fast response and high selectivity for HOCl over other various ROS or active reducing species but also the feasibility for the detection of HOCl over a broad pH range. The probe was successfully applied to the detection of HOCl fluctuations produced in macrophage cells. Additionally, with high physiological stability and excellent biocompatibility, the Pdot nanoprobe allowed for the visualization of LPS-induced HOCl generation in peritonitis of living mice. The dual-channel detection provided in vivo HOCl imaging with high contrast compared with the “off–on” imaging probes that can only be seen in a single detection channel once activated. These successful applications suggest that this versatile probe will be a promising and powerful tool in the investigations of the in situ HOCl status of diseases in living systems. We expect that the design strategy presented herein could be extended to construct other ratiometric fluorescent probes with precise and reliable measurement in biological systems.

## Supplementary Material

Refer to Web version on PubMed Central for supplementary material.

## Acknowledgments

We are grateful to the National Institutes of Health (CA186798, EB018831, MH113333), the Fred Hutchinson Cancer Research Center’s STTR program, and the University of Washington for support of this work.

## References

1. Diehn M, Cho RW, Lobo NA, Kalisky T, Dorie MJ, Kulp AN, Qian D, Lam JS, Ailles LE, Wong M, Joshua B, Kaplan MJ, Wapnir I, Dirbas FM, Somlo G, Garberoglio C, Paz B, Shen J, Lau SK, Quake SR, Brown JM, Weissman IL, Clarke MF. Nature. 2009; 458:780. [PubMed: 19194462]
2. Dröge W. Physiol. Rev. 2002; 82:47. [PubMed: 11773609]
3. Uttara B, Singh AV, Zamboni P, Mahajan RT. Curr. Neuropharmacol. 2009; 7:65. [PubMed: 19721819]
4. Hensley K, Robinson KA, Gabbita SP, Salsman S, Floyd RA. Free Radical Biol. Med. 2000; 28:1456. [PubMed: 10927169]
5. Valko M, Leibfritz D, Moncol J, Cronin MTD, Mazur M, Telser J. Int. J. Biochem. Cell Biol. 2007; 39:44. [PubMed: 16978905]
6. Fang FC. Nat. Rev. Microbiol. 2004; 2:820. [PubMed: 15378046]
7. Roos D, Winterbourn CC. Science. 2002; 296:669. [PubMed: 11976433]
8. Hawkins CL, Pattison DI, Davies MJ. Amino Acids. 2003; 25:259. [PubMed: 14661089]
9. Hawkins CL, Davies MJ. Chem. Res. Toxicol. 2002; 15:83. [PubMed: 11800600]

Author Manuscript Author Manuscript Author Manuscript Author Manuscript


10. Li H, Cao Z, Moore DR, Jackson PL, Barnes S, Lambeth JD, Thannickal VJ, Cheng G. Infect. Immun. 2012; 80:2528. [PubMed: 22526679]
11. Sakarya S, Gunay N, Karakulak M, Ozturk B, Ertugrul B. Wounds. 2014; 26:342. [PubMed: 25785777]
12. Pullar JM, Vissers MCM, Winterbourn CC. IUBMB Life. 2000; 50:259. [PubMed: 11327319]
13. Bhattacharyya A, Chattopadhyay R, Mitra S, Crowe SE. Physiol. Rev. 2014; 94:329. [PubMed: 24692350]
14. Chan J, Dodani SC, Chang CJ. Nat. Chem. 2012; 4:973. [PubMed: 23174976]
15. Li XH, Gao XH, Shi W, Ma HM. Chem. Rev. 2014; 114:590. [PubMed: 24024656]
16. Chen X, Wang F, Hyun JY, Wei T, Qiang J, Ren X, Shin I, Yoon J. Chem. Soc. Rev. 2016; 45:2976. [PubMed: 27092436]
17. Zhang Y-R, Chen X-P, Shao J, Zhang J-Y, Yuan Q, Miao J-Y, Zhao B-X. Chem. Commun. 2014; 50:14241.
18. Best QA, Sattenapally N, Dyer DJ, Scott CN, McCarroll ME. J. Am. Chem. Soc. 2013; 135:13365. [PubMed: 23889259]
19. Hou J-T, Li K, Yang J, Yu K-K, Liao Y-X, Ran Y-Z, Liu Y-H, Zhou X-D, Yu X-Q. Chem. Commun. 2015; 51:6781.
20. Zhou J, Li L, Shi W, Gao X, Li X, Ma H. Chem. Sci. 2015; 6:4884. [PubMed: 28717494]
21. Koide Y, Urano Y, Hanaoka K, Terai T, Nagano T. J. Am. Chem. Soc. 2011; 133:5680. [PubMed: 21443186]
22. Sun M, Yu H, Zhu H, Ma F, Zhang S, Huang D, Wang S. Anal. Chem. 2014; 86:671. [PubMed: 24308562]
23. Pu K, Shuhendler AJ, Rao J. Angew. Chem. Int. Ed. 2013; 52:10325.
24. Cheng G, Fan J, Sun W, Cao J, Hu C, Peng X. Chem. Commun. 2014; 50:1018.
25. Emrullahoglu M, Ucuncu M, Karakus E. Chem. Commun. 2013; 49:7836.
26. Wang B, Li P, Yu F, Song P, Sun X, Yang S, Lou Z, Han K. Chem. Commun. 2013; 49:1014.
27. Cao L, Zhang R, Zhang W, Du Z, Liu C, Ye Z, Song B, Yuan J. Biomaterials. 2015; 68:21. [PubMed: 26256295]
28. Li G, Lin Q, Sun L, Feng C, Zhang P, Yu B, Chen Y, Wen Y, Wang H, Ji L, Chao H. Biomaterials. 2015; 53:285. [PubMed: 25890727]
29. Zhang KY, Zhang J, Liu Y, Liu S, Zhang P, Zhao Q, Tang Y, Huang W. Chem. Sci. 2015; 6:301. [PubMed: 28757940]
30. Xiao Y, Zhang R, Ye Z, Dai Z, An H, Yuan J. Anal. Chem. 2012; 84:10785. [PubMed: 23190019]
31. Lee MH, Kim JS, Sessler JL. Chem. Soc. Rev. 2015; 44:4185. [PubMed: 25286013]
32. Wu P, Hou X, Xu J-J, Chen H-Y. Nanoscale. 2016; 8:8427. [PubMed: 27056088]
33. Ju E, Liu Z, Du Y, Tao Y, Ren J, Qu X. ACS Nano. 2014; 8:6014. [PubMed: 24873414]
34. Chen Z, Liu Z, Li Z, Ju E, Gao N, Zhou L, Ren J, Qu X. Biomaterials. 2015; 39:15. [PubMed: 25477167]
35. Wu X, Li Z, Yang L, Han J, Han S. Chem. Sci. 2013; 4:460.
36. Chen T, Hu Y, Cen Y, Chu X, Lu Y. J. Am. Chem. Soc. 2013; 135:11595. [PubMed: 23859158]
37. Peng H-S, Chiu DT. Chem. Soc. Rev. 2015; 44:4699. [PubMed: 25531691]
38. Yu J, Rong Y, Kuo C-T, Zhou X-H, Chiu DT. Anal. Chem. 2017; 89:42. [PubMed: 28105818]
39. Wu C, Chiu DT. Angew. Chem. Int. Ed. 2013; 52:3086.
40. Rong Y, Wu C, Yu J, Zhang X, Ye F, Zeigler M, Gallina ME, Wu IC, Zhang Y, Chan Y-H, Sun W, Uvdal K, Chiu DT. ACS Nano. 2013; 7:376. [PubMed: 23282278]
41. Yu J, Wu C, Zhang X, Ye F, Gallina ME, Rong Y, Wu IC, Sun W, Chan Y-H, Chiu DT. Adv. Mater. 2012; 24:3498. [PubMed: 22684783]
42. Sun W, Yu J, Deng R, Rong Y, Fujimoto B, Wu C, Zhang H, Chiu DT. Angew. Chem., Int. Ed. 2013; 52:11294.
43. Wu C, Hansen SJ, Hou Q, Yu J, Zeigler M, Jin Y, Burnham DR, McNeill JD, Olson JM, Chiu DT. Angew. Chem. Int. Ed. 2011; 50:3430.

Author Manuscript Author Manuscript Author Manuscript Author Manuscript


44. Ye F, Wu C, Jin Y, Chan Y-H, Zhang X, Chiu DT. J. Am. Chem. Soc. 2011; 133:8146. [PubMed: 21548583]
45. Zeigler MB, Sun W, Rong Y, Chiu DT. J. Am. Chem. Soc. 2013; 135:11453. [PubMed: 23895535]
46. Kuo C-T, Thompson AM, Gallina ME, Ye F, Johnson ES, Sun W, Zhao M, Yu J, Wu IC, Fujimoto B, DuFort CC, Carlson MA, Hingorani SR, Paguirigan AL, Radich JP, Chiu DT. Nat. Commun. 2016; 7:11468. [PubMed: 27118210]
47. Pu KY, Shuhendler AJ, Jokerst JV, Mei JG, Gambhir SS, Bao ZN, Rao JH. Nat. Nanotechnol. 2014; 9:233. [PubMed: 24463363]
48. Shuhendler AJ, Pu KY, Cui L, Uetrecht JP, Rao JH. Nat. Biotechnol. 2014; 32:373. [PubMed: 24658645]
49. Zhen X, Zhang CW, Xie C, Miao QQ, Lim KL, Pu KY. ACS Nano. 2016; 10:6400. [PubMed: 27299477]
50. Wang H, Li Y, Chen Y, Li L, Fang T, Tang Z. J. Mater. Chem. C. 2015; 3:5136.
51. Chan Y-H, Wu C, Ye F, Jin Y, Smith PB, Chiu DT. Anal. Chem. 2011; 83:1448. [PubMed: 21244093]
52. Wu IC, Yu J, Ye F, Rong Y, Gallina ME, Fujimoto BS, Zhang Y, Chan Y-H, Sun W, Zhou X-H, Wu C, Chiu DT. J. Am. Chem. Soc. 2015; 137:173. [PubMed: 25494172]
53. Liang L, Liu C, Jiao X, Zhao L, Zeng X. Chem. Commun. 2016; 52:7982.
54. Zhang W, Liu W, Li P, kang J, Wang J, Wang H, Tang B. Chem. Commun. 2015; 51:10150.
55. Zafarullah M, Li WQ, Sylvester J, Ahmad M. Cell. Mol. Life Sci. 2003; 60:6. [PubMed: 12613655]
56. Kettle AJ, Gedye CA, Winterbourn CC. Biochem. J. 1997; 321:503. [PubMed: 9020887]

Author Manuscript Author Manuscript Author Manuscript Author Manuscript

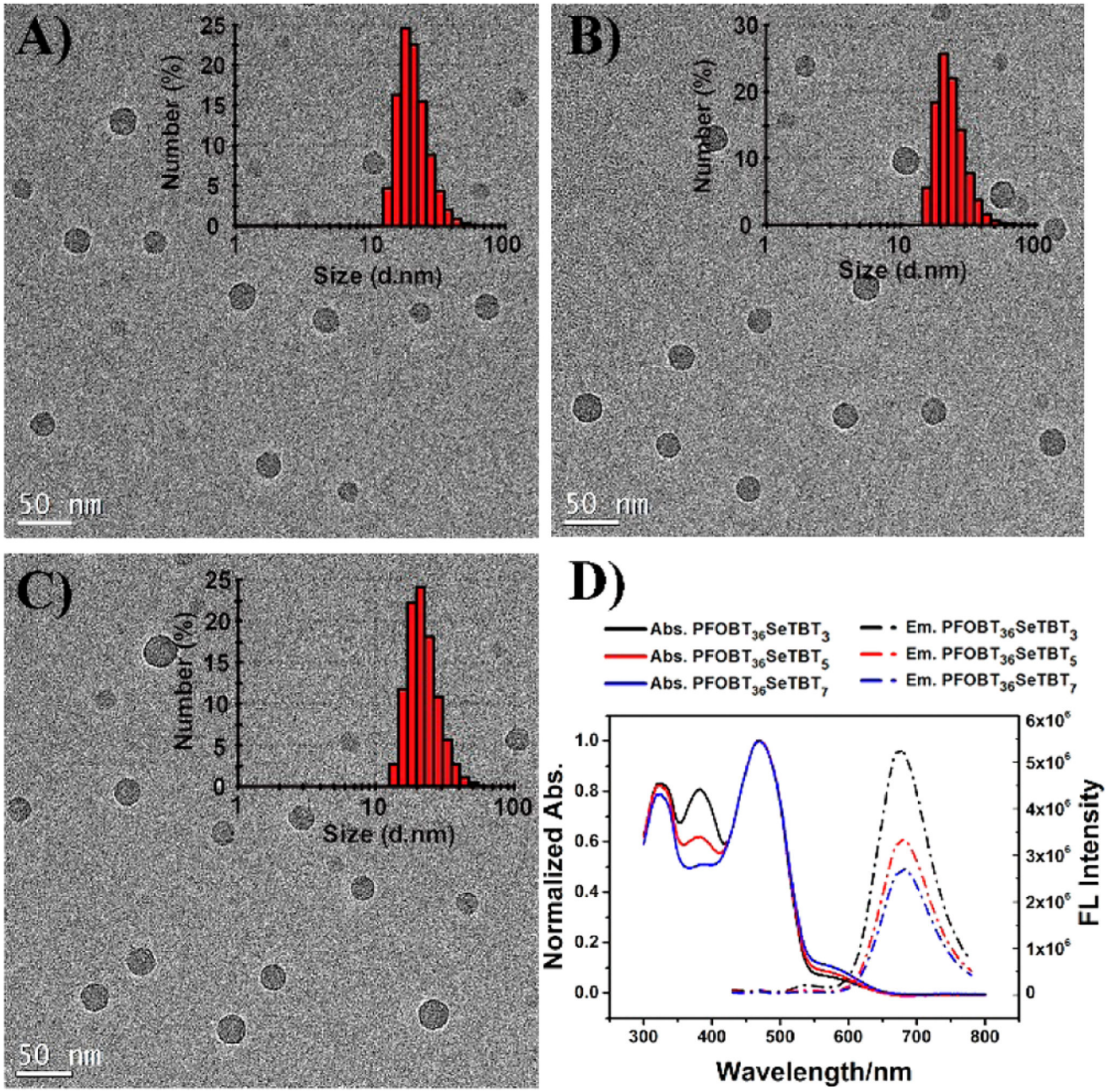


**Figure 1.**

Size and optical characterization of $PFOBT_{36}SeTBT_x$ Pdots. High-resolution TEM images of $PFOBT_{36}SeTBT_3$ Pdots (A), $PFOBT_{36}SeTBT_5$ Pdots (B), and $PFOBT_{36}SeTBT_7$ Pdots (C) (insets: DLS size distribution histograms of $PFOBT_{36}SeTBT_x$ Pdots). (D) Normalized absorption (Abs., solid line) and emission (Em., dashed line) spectra of $PFOBT_{36}SeTBT_x$ Pdots recorded at the concentration of 10 μg/mL in water (black line: $PFOBT_{36}SeTBT_3$ Pdots, red line: $PFOBT_{36}SeTBT_5$ Pdots, and blue line: $PFOBT_{36}SeTBT_7$ Pdots).

Author Manuscript Author Manuscript Author Manuscript Author Manuscript

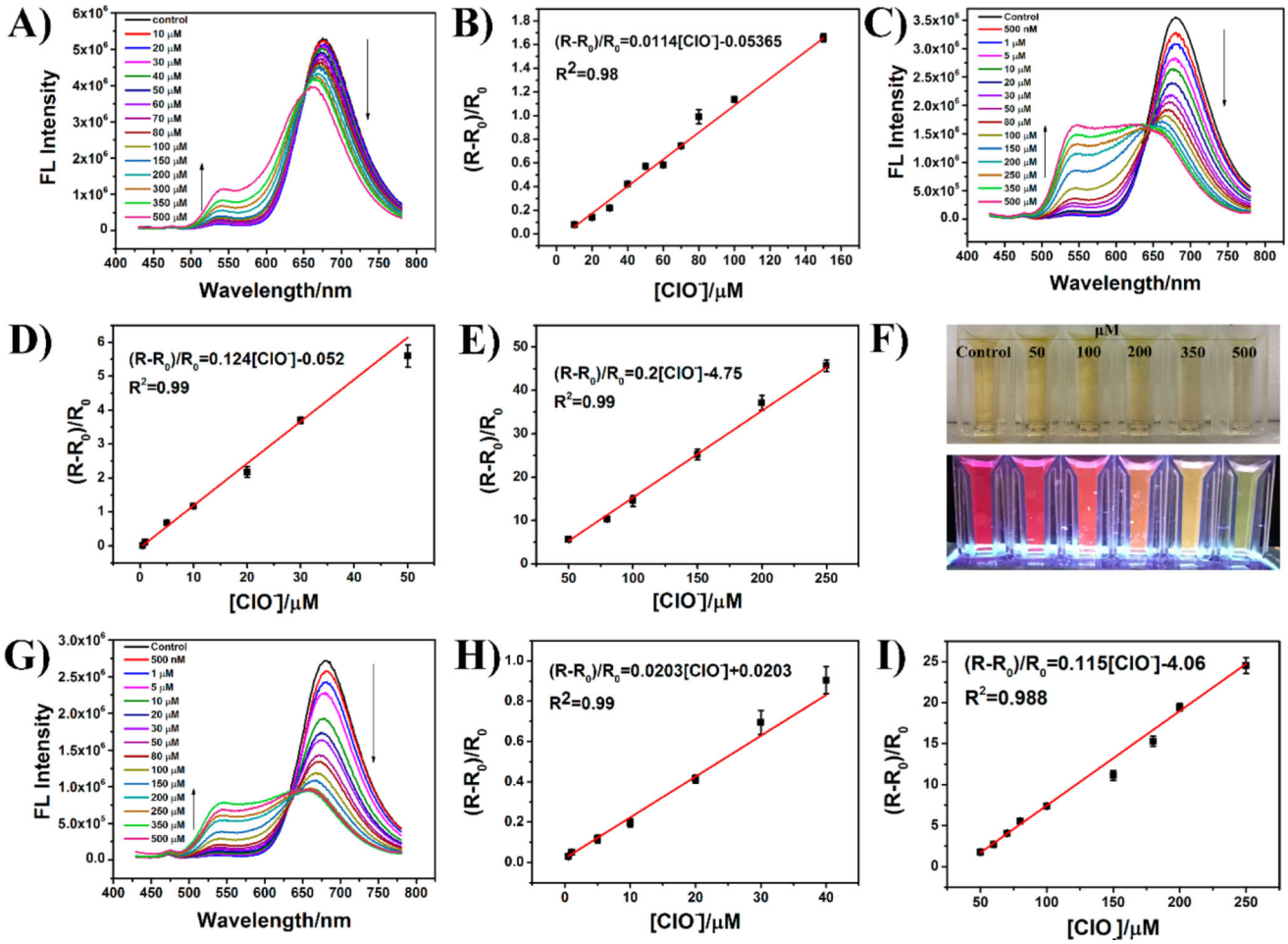


**Figure 2.**

Fluorescence performance and the linear relationship between the concentration of $ClO^-$ and the variation of the ratio ($R = I_{540nm}/I_{680nm}$; $R_0$ is the control of $PFOBT_{36}SeTBT_5$ Pdots without addition of $ClO^-$) of $PFOBT_{36}SeTBT_3$ (A, B), $PFOBT_{36}SeTBT_5$ (C–E), and $PFOBT_{36}SeTBT_7$ (G–I) Pdots in the presence of different concentrations of $ClO^-$ ions. (F) Photographs of $PFOBT_{36}SeTBT_5$ Pdots with the addition of $ClO^-$ taken under normal laboratory lighting and illumination with a UV light at 365 nm. All measurements were performed in 10 mM PBS solution (pH 7.4).

Author Manuscript Author Manuscript Author Manuscript Author Manuscript

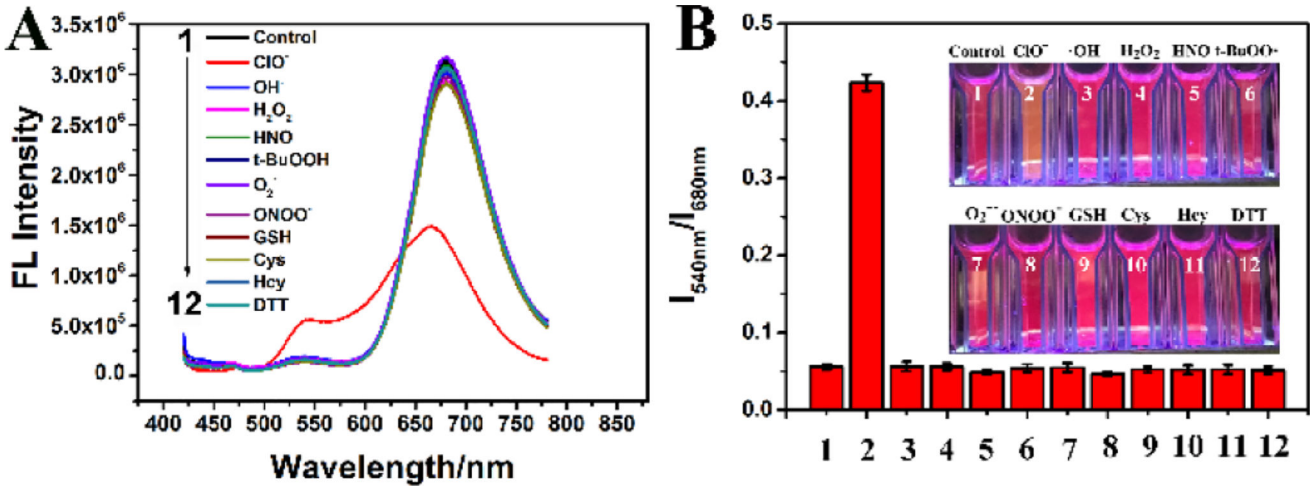


**Figure 3.**

Fluorescence spectra (A) and fluorescence intensity ratio (B) of $PFOBT_{36}SeTBT_5$ Pdots in the presence of various ROS and biologically relevant analytes: (1) PBS, (2) 100 μM $ClO^-$, (3) 1 mM $^{\bullet}OH$, (4) 1 mM $H_2O_2$, (5) 1 mM HNO, (6) 1 mM *t*-$BuOO^{\bullet}$, (7) 1 mM $O_2^{-\bullet}$, (8) 1 mM $ONOO^-$, (9) 1 mM GSH, (10) 1 mM Cys, (11) 1 mM Hcy, and (12) 1 mM DTT. Insets in (B) show the photos of $PFOBT_{36}SeTBT_5$ Pdots with the addition of various ROS and biologically relevant analytes taken under illumination with a UV light at 365 nm.

Author Manuscript Author Manuscript Author Manuscript Author Manuscript

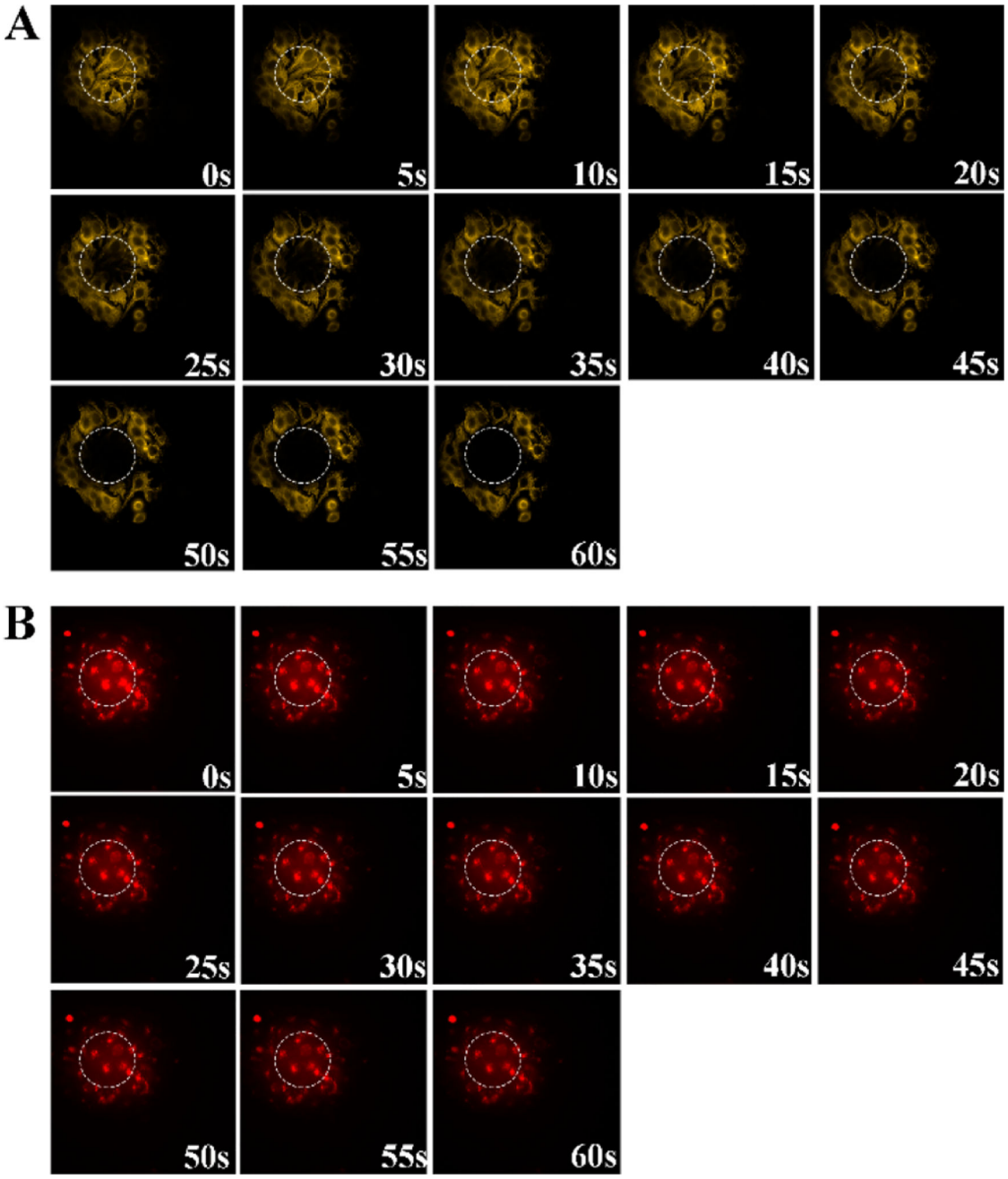


**Figure 4.**

Comparison of the photostabilities of phycoerythrin (PE) and $PFOBT_{36}SeTBT_5$ Pdots. Dynamic fluorescence images were taken by time-sequential scanning of MCF-7 cells incubated with PE-anticytokeratin (A) and $PFOBT_{36}SeTBT_5$ Pdots (B). The dotted circles indicate the laser spot, which is the region of irradiation.

Author Manuscript Author Manuscript Author Manuscript Author Manuscript

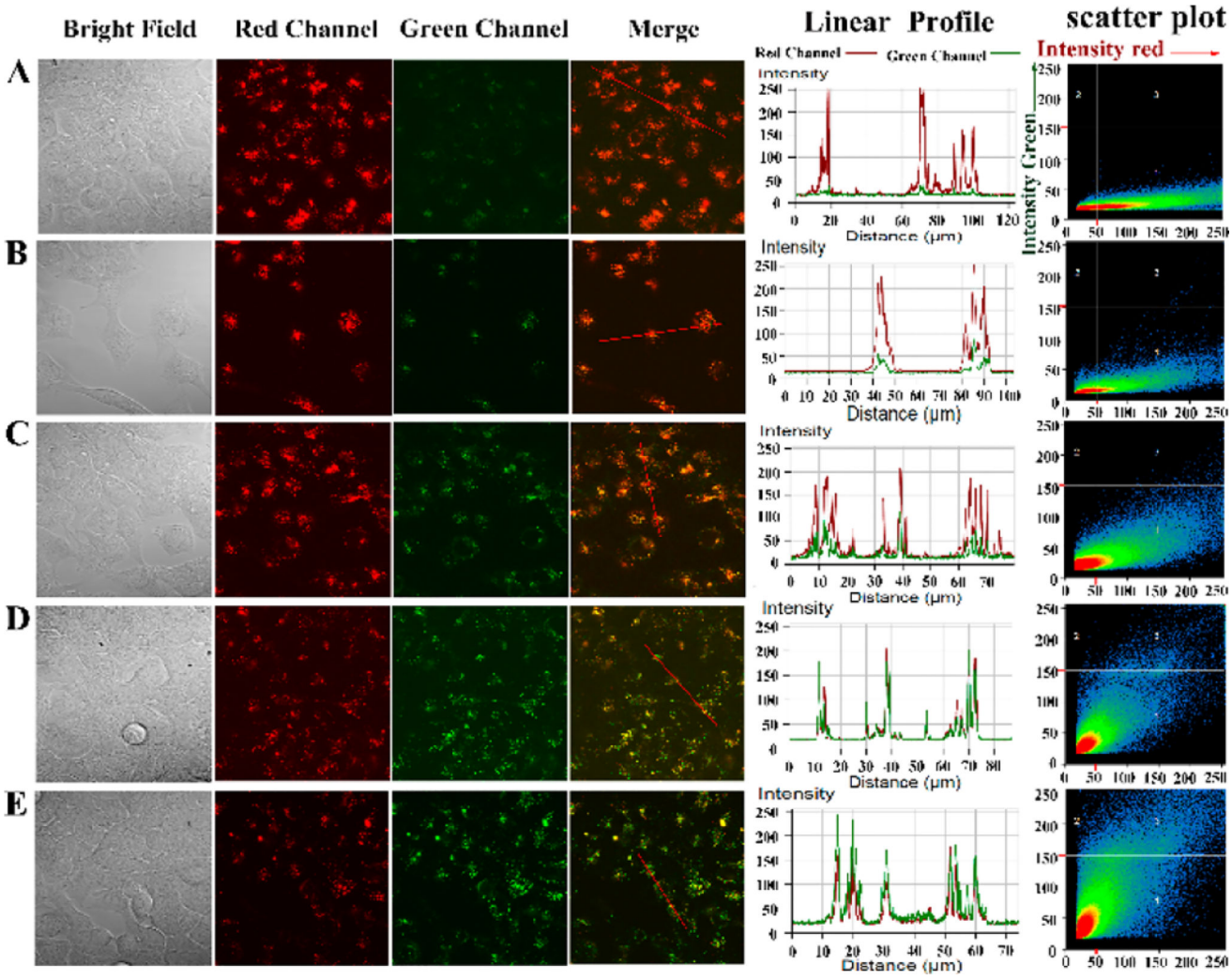


**Figure 5.**

Confocal fluorescence imaging of exogenous $ClO^-$ in MCF-7 cells. MCF-7 cells were first incubated with $PFOBT_{36}SeTBT_5$ Pdots (10 μg/mL) overnight at 37 °C and then were incubated with different solutions for 30 min: (A) PBS solution; (B) 10 μM NaClO; (C) 25 μM NaClO; (D) 50 μM NaClO; and (E) 80 μM NaClO. Fluorescence images were acquired using a confocal microscope with 405 nm excitation and fluorescence emission windows of green channel (530–600 nm) and red channel (>650 nm).

Author Manuscript Author Manuscript Author Manuscript Author Manuscript

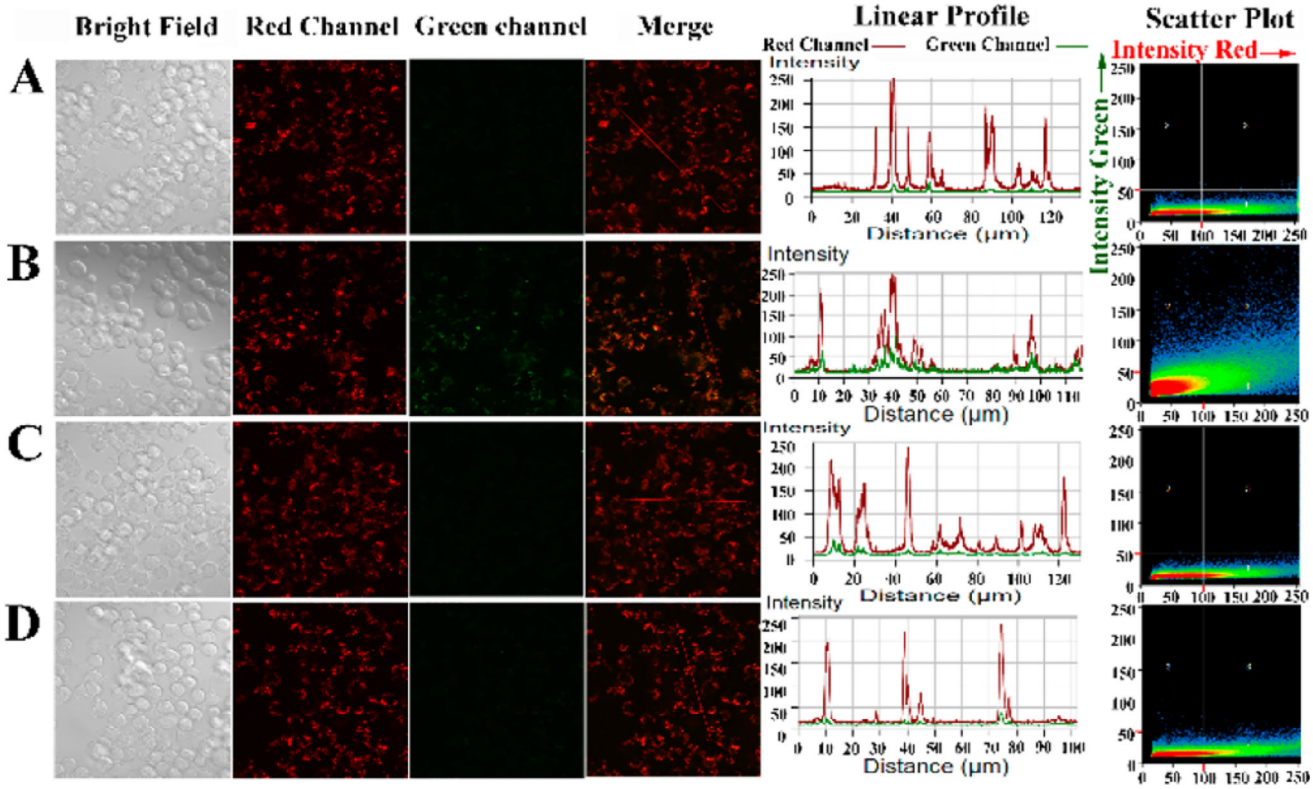


**Figure 6.**

Confocal fluorescence imaging of endogenous $ClO^-$ in stimulated RAW 264.7 macrophages incubated with $PFOBT_{36}SeTBT_5$ Pdots (10 μg/mL, 4 h) before imaging: (A) nontreated cells; (B) cells successively treated with LPS (4 h) and PMA (0.5 h); (C) cells pretreated with NAC 2 h before treated with LPS (4h) and PMA (0.5 h), followed with NAC for 1 h; and (D) cells pretreated with ABAH 2 h before treated with LPS (4 h) and PMA (0.5 h), followed with ABAH for 1 h. [LPS] = 1 μg/mL; [PMA] = 5 μg/mL; [NAC] = 1 mM; [ABAH] = 1 mM. Green channel at 530–600 nm; far-red channel at >650 nm.

Author Manuscript Author Manuscript Author Manuscript Author Manuscript

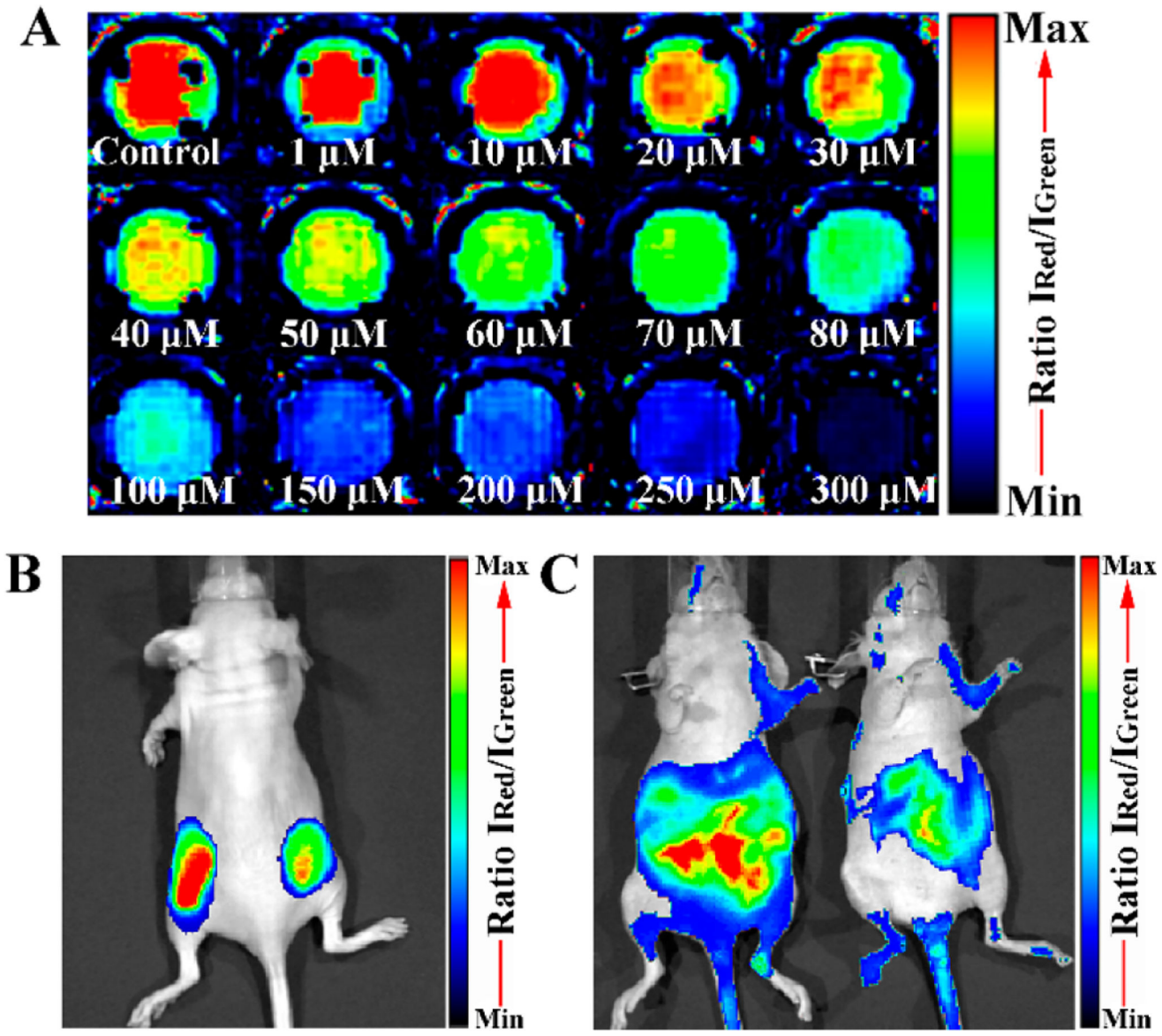


**Figure 7.**

(A) Ratiometric images (pseudocolor) of $PFOBT_{36}SeTBT_5$ Pdots in 96-well plate treated with different concentrations of $ClO^-$ using an in vivo imaging system; (B) In vivo imaging of exogenous $ClO^-$ using $PFOBT_{36}SeTBT_5$ Pdots. Representative ratiometric (pseudocolor) image of mouse with the subcutaneous implantation of $PFOBT_{36}SeTBT_5$ Pdots (0.1 mg/mL, 0.1 mL) (left) and $PFOBT_{36}SeTBT_5$ Pdots (0.1 mg/mL, 0.1 mL) + $ClO^-$ (10 nmol) (right). (C) In vivo imaging of endogenous $ClO^-$ production from the peritoneal cavity of the mice with PFOBT36SeTBT5 Pdots during an LPS-mediated inflammatory response. Representative ratiometric images (pseudocolor) of mice intraperitoneally treated with saline (left) and LPS (right), followed by an intraperitoneal injection of $PFOBT_{36}SeTBT_5$ Pdots (0.3 mg/mL, 0.2 mL) 4 h later. Fluorescence images were acquired 30 min after the injection of Pdots with a 465 nm excitation filter and 540 nm (green channel) and 680 nm (red

channel) emission filters. Ratiometric images were obtained by pixelby-pixel calculation using ImageJ software.

Author Manuscript Author Manuscript Author Manuscript Author Manuscript

Author Manuscript Author Manuscript Author Manuscript Author Manuscript

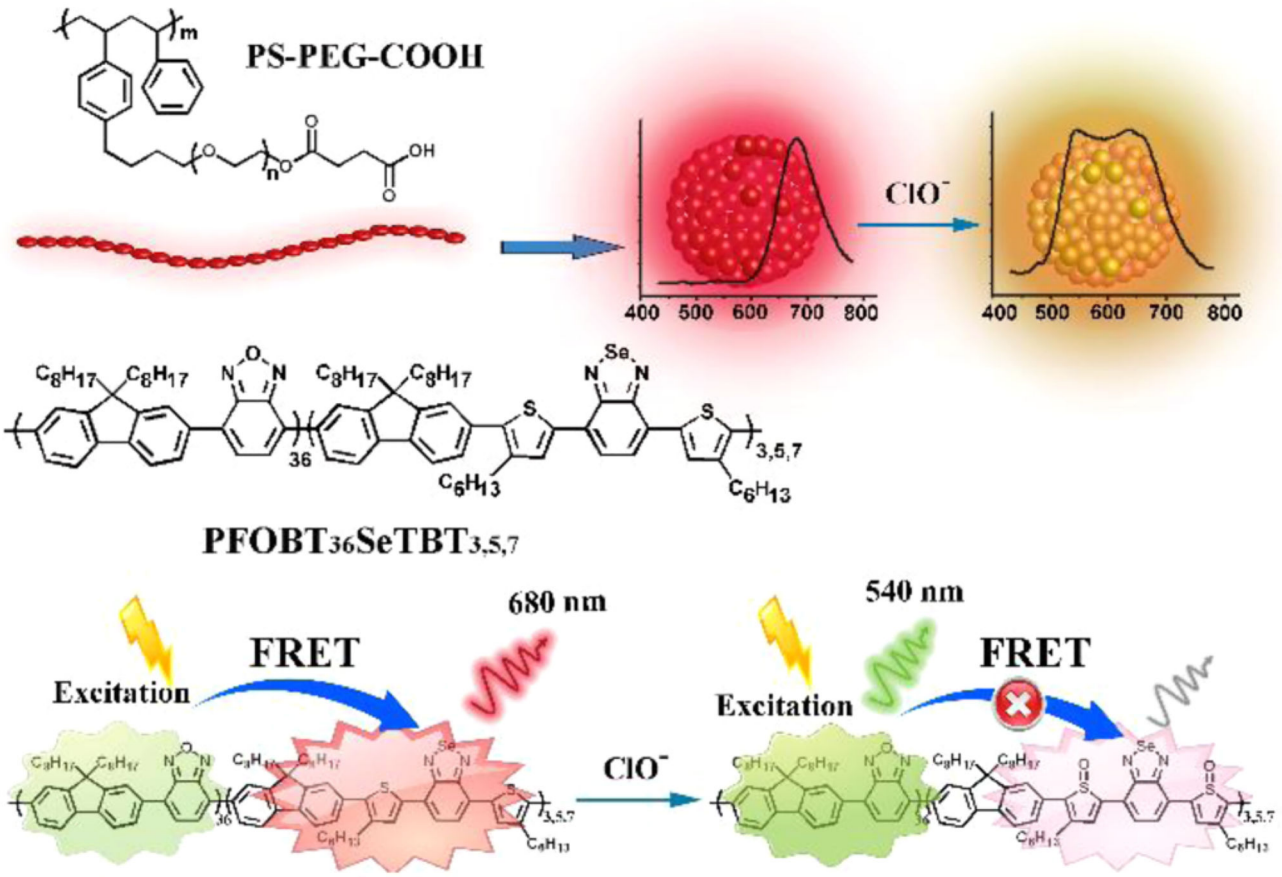


**Scheme 1.**

Schematic Illustration of Pdot Preparation by Nanoprecipitation and Hydrocholorous Acid Sensing